THE JOURNAL OF BIOLOGICAL CHEMISTRY VOL. 284, NO. 22, pp. 15184–15192, May 29, 2009

Molecular Basis of Coiled Coil Coactivator Recruitment by the Aryl Hydrocarbon Receptor Nuclear Translocator (ARNT)*[S]

Received for publication, November 6, 2008, and in revised form, March 13, 2009 Published, JBC Papers in Press, March 26, 2009, DOI 10.1074/jbc.M808479200

Carrie L. Partch[‡1], **Paul B. Card**[‡], **Carlos A. Amezcua**[‡], **and Kevin H. Gardner**[‡§2]

From the Departments of [‡]*Biochemistry and* [§]*Pharmacology, University of Texas Southwestern Medical Center at Dallas, Dallas, Texas 75390*

The aryl hydrocarbon receptor nuclear translocator (ARNT) serves as the obligate heterodimeric partner for bHLH-PAS proteins involved in sensing and coordinating transcriptional responses to xenobiotics, hypoxia, and developmental pathways. Although its C-terminal transactivation domain is dispensable for transcriptional activation *in vivo*, ARNT has recently been shown to use its N-terminal bHLH and/or PAS domains to interact with several transcriptional coactivators that are required for transcriptional initiation after xenobiotic or hypoxic cues. Here we show that ARNT uses a single PAS domain to interact with two coiled coil coactivators, TRIP230 and CoCoA. Both coactivators interact with the same interface on the ARNT PAS-B domain, located on the opposite side of the domain used to associate with the analogous PAS domain on its heterodimeric bHLH-PAS partner HIF-2α. Using NMR and biochemical studies, we identified the ARNT-interacting motif of one coactivator, TRIP230 as an L*XX*LL-like nuclear receptor box. Mutation of this motif and proximal sequences disrupts the interaction with ARNT PAS-B. Identification of this ARNT-coactivator interface illustrates how ARNT PAS-B is used to form critical interactions with both bHLH-PAS partners and coactivators that are required for transcriptional responses.

PAS (Per-ARNT-Sim)[3] domains are small, modular domains that mediate interactions with proteins (and often small molecule ligands) to coordinate cellular responses to diverse environmental stimuli (1). The largest class of eukaryotic PAS-containing proteins are transcription factors containing a basic helix-loop-helix (bHLH) DNA-binding domain followed by two PAS domains, known as the bHLH-PAS family (2). As functional heterodimers, bHLH-PAS complexes bind DNA at specific promoter elements and recruit transcriptional coactivators via their C-terminal transactivation domains (TADs) to regulate transcriptional responses to diverse stimuli. In particular, the ubiquitously expressed protein ARNT is of central importance within the bHLH-PAS family, acting as the obligate heterodimeric partner for the aryl hydrocarbon receptor (AHR), hypoxia-inducible factor-α (HIF-α), and single-minded (SIM) to regulate transcriptional responses to xenobiotics, hypoxia, and neurogenesis, respectively (3). ARNT heterodimeric complexes are involved in the etiology and progression of many forms of human cancer through the metabolic activation of dietary and environmental carcinogens (AHR·ARNT) and the adaptation of solid tumors to chronic hypoxia (HIF-α·ARNT, also known as HIF) (4, 5).

Heterodimerization of bHLH-PAS proteins is mediated by contacts between both the bHLH and the tandem PAS domains, with inter-PAS domain contacts playing a critical role in the specificity and stability of heterodimer formation (Fig. 1*A*) (6–9). Structures of the HIF-2α·ARNT PAS-B heterodimer demonstrate that the two PAS-B domains associate via their β-sheets (Refs. 10, 11 and Fig. 1*B*) and disruption of this interface by point mutations significantly attenuates the transcriptional response to hypoxia by destabilizing the full-length heterodimer complex (8, 9). In addition to forming stable complexes on specific DNA promoters, bHLH-PAS heterodimers must also recruit transcriptional coactivators, a diverse pool of proteins that are required for histone modification and/or recruitment of general transcriptional machinery. The dynamic association of coactivators with sequence-specific transcription factors allows the temporal- and tissue-specific modulation of transcription, as well as influencing the specificity of target gene induction (reviewed in Ref. 12).

The use of glutamine-rich C-terminal TADs by HIF-α and AHR to recruit coactivators is well documented (13–15), though the ARNT C-terminal glutamine-rich domain is apparently dispensable for coactivator recruitment *in vivo* (16, 17). The recent discovery of coiled coil coactivators that target domains other than the C-terminal TADs establishes that multiple structural motifs are used by bHLH-PAS proteins to recruit coactivators (18–21). Domain-swapping studies have shown that PAS domains within the bHLH-PAS family contribute to the specificity of target gene induction, suggesting that PAS domains themselves participate in the recruitment of specific coactivators (22). Two candidates for such PAS-directed coactivators are CoCoA (coiled coil coactivator) (20) and TRIP230 (thyroid hormone receptor/retinoblastoma-interacting protein 230, also known as TRIP11) (18), which appear to interact with the N-terminal bHLH and/or PAS domains of

* This work was supported, in whole or in part, by National Institutes of Health Grants GM081875 (to K. H. G.) and CA130441 (to C. L. P.).

[S] The on-line version of this article (available at http://www.jbc.org) contains supplemental Figs. S1–S6.

[1] Supported by a fellowship from the Chilton/Bell Foundation.

[2] To whom correspondence should be addressed: 5323 Harry Hines Blvd. Dallas, TX 75390-8816. Fax: 214-645-6353; E-mail: Kevin.Gardner@utsouthwestern.edu.

[3] The abbreviations used are: PAS, Per-ARNT-Sim; bHLH, basic helix-loop-helix; ARNT, aryl hydrocarbon receptor nuclear translocator; HIF-α, hypoxia-inducible factor α; HSQC, heteronuclear single quantum coherence; GST, glutathione *S*-transferase; WT, wild type; NOESY, nuclear Overhauser effect spectroscopy; CoCoA, coiled coil coactivator; TRIP230, thyroid hormone receptor/retinoblastoma-interacting protein 230; AINT, ARNT-interacting protein; NR box, nuclear receptor box; MES, 4-morpholineethanesulfonic acid.

ARNT. TRIP230 is recruited to endogenous promoters after hypoxia or xenobiotic stress and is required for the function of ARNT heterodimers *in vivo* (18), highlighting the previously unappreciated role of the N-terminal domains of ARNT in transcriptional regulation.

In this study, we investigate the molecular basis for the interaction of ARNT with coiled coil coactivators. We demonstrate that the coiled coil coactivators TRIP230 and CoCoA bind a similar interface on ARNT that maps to the α-helical face of PAS-B. Our data suggest an unrecognized commonality in PAS domain interactions, because an analogous interface has been described for the interaction the PAS-B domain of the SRC-1 coactivator with several helical targets, mediated by an L*XX*LL motif (L is Leu; *X* is any amino acid) (23, 24). Notably, detailed characterization of the ARNT-interacting sequence on TRIP230 revealed that an L*XX*LL-like motif is critical for the interaction, demonstrating functional similarities in recruitment of helical targets by PAS domains. Collectively, these data point to a model of simultaneous engagement of bHLH-PAS heterodimeric partners and coactivators by ARNT PAS-B.

EXPERIMENTAL PROCEDURES

Protein Expression and Purification—The cloning and purification of ARNT PAS-B and HIF-2α PAS-B have been described elsewhere (8, 10). PCR-generated DNA fragments were subcloned into the following Parallel bacterial expression vectors (25, 26): pHis$_6$Gβ1-ARNT PAS-A (residues 155–350), pHis$_6$-ARNT PAS-AB (residues 155–470), and coiled coil coactivator truncations (TRIP230 and CoCoA) were all subcloned into the pGST-parallel vector. Mutations were introduced by PCR, and all constructs were verified by DNA sequencing.

Proteins were expressed in *Escherichia coli* strain BL21(DE3) (Novagen). Isotopically labeled proteins were prepared using M9 minimal medium containing $^{15}NH_4Cl$ and [$^{13}C_6$]glucose as the sole nitrogen and carbon sources, respectively. ARNT PAS domains were expressed as His$_6$ or His$_6$Gβ1 fusions and purified from bacterial lysate by Ni^{2+}-Sepharose (GE Healthcare) affinity chromatography. The His$_6$ tag was cleaved from U-^{15}N His$_6$-ARNT PAS-B for NMR spectroscopy by incubating overnight with His$_6$-TEV (Tobacco Etch Virus) protease (27), followed by Ni^{2+}-Sepharose and gel filtration (Superdex 75) chromatography, resulting in purified U-^{15}N ARNT PAS-B with 4 vector-derived N-terminal residues (GAMD). All coactivator fragments were expressed as GST fusions and purified from bacterial lysate by glutathione-Sepharose (GE Healthcare) affinity chromatography. Proteins were cleaved overnight with His$_6$-TEV, followed by Ni^{2+}-Sepharose and either gel filtration (Superdex 75) or cation exchange (Mono S) chromatographies to remove the protease and GST, respectively. Purified coactivator fragments contain a 17-residue vector-derived N-terminal sequence (GAMDPEFKGLRRRAQLV). All protein concentrations were determined by absorbance at 280 nm using predicted extinction coefficients (in M^{-1} cm^{-1}) of: His$_6$GB1-ARNT PAS-A, 33,265; His$_6$-ARNT PAS-B, 21,680; ARNT PAS-B, 15,720; His$_6$-ARNT PAS-AB, 37,650; HIF-2α PAS-B, 17,670; TRIP230$^{1583-1688}$, 2,980; CoCoA$^{407-535}$, 12,490; and TRIP230$^{1583-1620}$, 1490 (28).

Pull-down Assays—Soluble *E. coli* lysate expressing GST-tagged coactivator fragments was generated by lysing cells in phosphate-buffered saline (10 mM sodium/potassium phosphate, pH 7.4, 137 mM NaCl, 2.7 mM KCl) by high-pressure extrusion, followed by centrifugation at 20,000 × *g* for 30 min at 4 °C. Glycerol was added to a final concentration of 8% (v/v) to the supernatant, and aliquots were quick frozen in liquid nitrogen for storage at −80 °C. Overexpression of GST-tagged fragments within soluble extracts was analyzed by SDS-PAGE to estimate equal input for pull-down assays. Equal amounts of GST-tagged coactivator fragments were incubated with 12 μl of Ni^{2+}-Sepharose beads (GE Healthcare) in binding buffer (50 mM Tris, pH 7.5, 150 mM NaCl, 20 mM imidazole, 5 mM β-mercaptoethanol) in the presence or absence of 2 μM His$_6$-tagged ARNT PAS domain constructs (0.03–0.07 mg/ml) in a total volume of 400 μl for 4–16 h at 4 °C. Beads were washed twice with 400 μl of binding buffer and eluted with 8 μl of 4× SDS Laemmli buffer. Samples were resolved on a 10% Bis-Tris NuPAGE gel run with 1× MES resolving buffer (Invitrogen) and Coomassie Blue-stained for detection of bound proteins.

Circular Dichroism Spectroscopy—Protein samples were buffer-exchanged into 10 mM sodium phosphate, pH 6.5, 17 mM NaCl. All spectra were collected with 15 μM protein concentrations (ranging from 0.09 to 0.2 mg/ml) on an Aviv 62D Spectropolarimeter at 25 °C using a 0.1-cm path length quartz cuvette, recording every 1.0 nm between 190 and 260 nm. The reference signal from buffer was subtracted from all spectra, which represent the mean of three independent scans. Molar residue ellipticities were calculated from raw ellipticities (mdeg) using Equation 1.

$$\theta\ (\mathrm{deg \cdot cm^2/dmol \cdot res}) = (\mathrm{mdeg})(\mathrm{conc\ protein\ (M)})^{-1} \cdot (0.1\ \mathrm{cm})^{-1} \cdot (10\ \mathrm{dmol})^{-1} \cdot (\#\ \mathrm{residues})^{-1} \quad \text{(Eq. 1)}$$

NMR Spectroscopy—All NMR experiments were performed at 25 °C on Varian INOVA 600 or 800 MHz spectrometers equipped with ^{1}H,^{13}C,^{15}N indirect detection triple resonance probes and a Z-axis pulsed field gradient. ^{15}N/^{1}H HSQC titration experiments of 200 μM U-^{15}N ARNT PAS-B were carried out by the stepwise addition of natural abundance Trip230$^{1583-1688}$ or CoCoA$^{407-535}$ (50–300 μM over 4 steps); samples were buffer-exchanged to 50 mM Tris, pH 7.5, 17 mM NaCl, 5 mM dithiothreitol, concentrated to 500 μl using an Amicon stirred cell concentrator with a 10 kDa MWCO filter, and D_2O was added to a final concentration of 10% (v/v). Differential broadening analysis was performed in NMRView (29) by obtaining the ratio of intensities of well-resolved ARNT PAS-B peaks in the presence and absence of coactivator fragments; residues broadened $> 1\sigma$ beyond the mean were mapped on the ARNT PAS-B structure (PDB 1X0O) (10). ^{15}N/^{1}H HSQC titration experiments of 100 μM U-^{15}N TRIP230$^{1583-1620}$ were carried out by stepwise addition of ARNT or HIF-2α PAS-B (50–900 μM in 6 steps) in 50 mM MES pH 6.5, 17 mM NaCl, 5 mM dithiothreitol, and a 3-kDa MWCO filter was used during concentration. Significantly perturbed residues for which the $\Delta\delta_{TOT} > 0.05$ ppm were obtained using Equation 2,

$$\Delta\delta_{TOT} = [(\Delta\delta^1\mathrm{H})^2 + (\chi \times \Delta\delta^{15}\mathrm{N})^2]^{1/2} \quad \text{(Eq. 2)}$$

normalized for proton with the scale factor $\chi = 0.17$, established from estimates of atom-specific chemical shift ranges in a protein environment (30).

Chemical shift assignment of 400 μM U-^{15}N/^{13}C TRIP230$^{1583-1620}$ was obtained from standard triple resonance experiments as follows. Backbone resonances were manually assigned using heteronuclear ^{15}N/^{1}H HSQC, HNCA, HNCACB, CBCA(CO)NH, and HNCO, and side-chain resonances were assigned from HCCH-TOCSY, HC(CO)NH-TOCSY, C(CO)NH-TOCSY (31), and a three-dimensional simultaneously ^{13}C,^{15}N-edited NOESY spectrum (32). Spectra were processed using NMRPipe (33) and analyzed with NMRView (29).

Sequence Alignment—Protein sequences used for the TRIP230 alignment by CLUSTAL-W2 (34) were obtained from the NCBI Protein Data Base: *Homo sapiens* NP_004230, *Mus musculus* XP_917811, *Gallus gallus* XP_421324, *Anopheles gambiae* XP_311743, *Drosophila melanogaster* NP_788907, and *Tribolium castaneum* XP_967067.

AlphaScreen® Assay—Binding affinities for GST coactivators and ARNT PAS-B-FLAG were determined by AlphaScreen® assay using glutathione donor beads and FLAG acceptor beads according to the manufacturer's instructions (PerkinElmer Life Sciences). Briefly, purified GST coactivators were titrated from either 12.5 nM to 1.6 μM (GST-TRIP230$^{1583-1688}$ or GST alone) or 0.8 μM to 51 μM (GST-TRIP230$^{1583-1688}$ Site 1, GST-TRIP230$^{1593-1688}$, or GST alone) in triplicate in the presence or absence of 25 nM ARNT PAS-B-FLAG. Donor and acceptor beads were added (50 nl/well) in 50 mM Tris, pH 7.5, 100 mM NaCl, 1 mM dithiothreitol for a total volume of 25 μl in an Opti-Plate 384 well plate. The plate was read after 4 h of incubation in the dark at RT by a Wallac EnVision 2100 (PerkinElmer Life Sciences). Binding affinities were calculated by nonlinear regression using an equation for simple one site binding (GraphPad Prism 5.0a).

RESULTS

ARNT PAS-B Is the Primary Site of Coiled Coil Coactivator Binding—Prior biochemical studies on the ARNT binding abilities of several coiled coil coactivators identified large fragments required for interaction. An ARNT-interacting region of 133 residues was identified for TRIP230 spanning residues 1583–1716 in the conserved C-terminal domain, near its thyroid hormone receptor-binding L*XX*LL motif (18, 35). The ARNT interaction site was not defined on the 631-residue CoCoA protein (20); however, a central coiled coil region critical for interaction with the bHLH-PAS domains of the GRIP1 coactivator is predicted to contain two distinct coiled coil regions (36). Based on these predictions, we subcloned both coiled coil regions to determine their interaction with ARNT by pull-down assay and identified residues 407–514 as the ARNT-interacting motif in CoCoA (data not shown).

To complement these data with higher resolution identification of the coiled coil coactivator-interacting regions of ARNT, we purified both His$_6$-tagged ARNT PAS domains alone and in tandem for use in pull-down assays with GST-tagged coactivators (Fig. 1*C*). ARNT PAS-A is considerably larger than PAS-B because of the presence of several long loops compared with the canonical PAS domain, and care was taken during subcloning to maintain the required secondary structure elements of the PAS fold. An examination of all purified PAS domains by ^{15}N/^{1}H HSQC spectra demonstrated excellent ^{1}H chemical shift dispersion consistent with well-folded PAS domains (data not shown). Purified His$_6$-tagged PAS domains were incubated with *E. coli* lysates containing overexpressed GST-tagged coactivator fragments or GST alone, and binding was assessed by pull-down assay using Ni^{2+}-Sepharose. ARNT PAS-B, but not the isolated PAS-A domain, interacted directly with fragments of either TRIP230 or CoCoA (Fig. 1*D*). Moreover, the tandem PAS-AB fragment bound equivalent amounts of both coiled coil coactivators as the PAS-B domain alone, suggesting that it is unlikely that the PAS-A domain has a high affinity secondary binding site on the PAS-A domain that cooperatively recruits coiled coil coactivators. Therefore, ARNT PAS-B domain is the primary site of interaction for both TRIP230 and CoCoA.

Mapping Coiled Coil Coactivator Binding on ARNT PAS-B by NMR—We then performed NMR titration experiments to map the binding region of coiled coil coactivators onto the ARNT PAS-B domain. 200 μM uniformly ^{15}N-labeled PAS-B (U-^{15}N PAS-B) was incubated with increasing concentrations of TRIP230 residues 1583–1688 (subsequently denoted TRIP230$^{1583-1688}$) (50–300 μM) and binding was monitored by ^{15}N/^{1}H HSQC spectra. Signals for several ^{15}N-PAS-B amides began broadening early in the titration, suggesting that the kinetics of interaction are in the slow-intermediate exchange regime, where peaks at the interface of the two proteins significantly broaden with respect to the rest of the protein. Differential broadening analysis was done to map the coactivator binding site on ARNT PAS-B by comparing the ratio of peak intensities for all well-resolved PAS-B peaks in the presence and absence of 100 μM TRIP1230$^{1583-1688}$ to the mean intensity for all peaks (Fig. 2*A*). Significantly broadened peaks were found throughout the primary sequence and plotted onto the structure of ARNT PAS-B (Fig. 2*B*), mapping to the α-helical face of the domain. The NMR titration experiments were repeated with CoCoA$^{407-535}$ and a similar interface was identified (Fig. 2*C*). In contrast, the interaction of ARNT PAS-B with HIF-2α PAS-B selectively perturbs residues located on the opposite side of the protein on the β-sheet (Fig. 2*D* and Ref. 10), demonstrating that interaction with coactivators and HIF-2α occur on opposite sides of the ARNT PAS-B domain.

Mutation of ARNT α-Helical Residues Disrupts Interaction with TRIP230 but Not HIF-2α PAS-B—We then mutated a subset of residues on the ARNT α-helical face that were significantly broadened by interaction with both coactivators (Fig. 2*E*) to disrupt the interaction. Purified His$_6$-tagged WT or mutant PAS-B domains were incubated with *E. coli* lysates containing overexpressed GST-TRIP$^{1583-1688}$ and binding was monitored by pull-down assay (Fig. 2*F*). Mutations for I369A, V397A, and K419A, either singly or in combination, partially disrupted the interaction with GST-TRIP$^{1583-1688}$. We then tested whether the ARNT PAS-B I369A/V397A double mutant could still interact with HIF-2α PAS-B, which utilizes the opposing β-sheet interface (10). The ^{15}N/^{1}H HSQC spectrum of I369A/V397A displayed minimal chemical shift perturbations that were localized to the α-helical surface (supplemental Fig. S1).

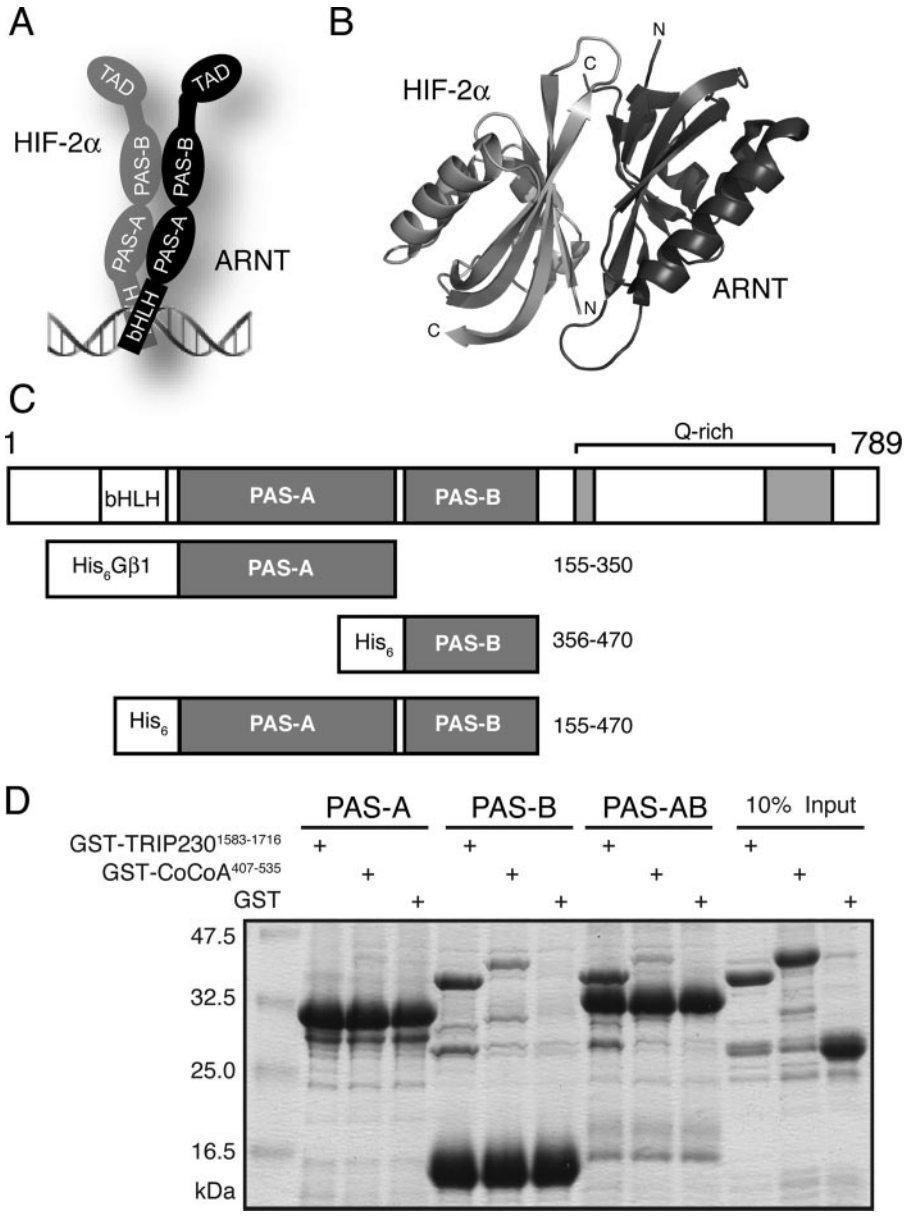

FIGURE 1. **ARNT PAS domains: structure and interaction with coiled coil coactivators.** *A*, schematic model of bHLH-PAS heterodimer bound to DNA. *B*, structure of HIF-2α PAS-B·ARNT PAS-B heterodimer (PDB 3F1P (11)), HIF-2α (*light gray*), ARNT (*dark gray*). *C*, schematic representation of ARNT domain structure. Full-length protein shown above, with expression constructs for isolated or tandem PAS domains shown below. *D*, pull-down assay of His_6-tagged ARNT PAS domains with GST-tagged coactivators. Bound proteins were analyzed by Coomassie Blue stain of SDS-PAGE. MW of ARNT PAS constructs: His_6Gβ1 ARNT PAS-A, 32.0 kDa; His_6 ARNT PAS-B, 13.6 kDa; His_6 ARNT PAS-AB, 35.6 kDa.

As shown in Fig. 2*G*, both WT and I369A/V397A ARNT PAS-B domains exhibited similar HIF-2α-induced chemical shift perturbations consistent with binding of the HIF-2α PAS-B on the intermediate-fast exchange timescale as previously described (10). Therefore, mutation of the ARNT PAS-B α-helical face selectively disrupts interaction with coactivators.

Identifying a Minimal Interacting Region of TRIP230—We subsequently chose to focus on TRIP230 to characterize the ARNT-interacting motif because it is required for transcriptional responses by both AHR·ARNT and HIF-α·ARNT complexes and interacts exclusively with ARNT within the bHLH-PAS family (18). Our initial mapping studies showed that a very C-terminal fragment of the TRIP230 ARNT-interacting motif spanning residues 1663–1716 (18) was not required for interaction with ARNT PAS-B (supplemental Fig. S2). Furthermore, other constructs containing N-terminal extensions beyond residue 1583 had no additional effect on ARNT PAS-B binding (data not shown). We then made a series of truncations of the remaining fragment based on secondary structure and coiled coil predictions (Fig. 3*A*) and performed pull-down assays with His_6-ARNT PAS-B to qualitatively determine which fragments retained binding to the PAS-B domain. The N-terminal segment containing residues 1583–1620 retained its interaction with PAS-B, while the C-terminal fragment did not (Fig. 3*B*). Surprisingly, a truncation eliminating 10 residues with no predicted secondary structure (residues 1583–1593) significantly decreased binding to ARNT PAS-B, demonstrating the importance of these residues for interaction with ARNT.

Structural Characteristics of the Minimal TRIP230 Peptide—We obtained circular dichroism spectra to determine the secondary structure of the minimal TRIP230 peptide comprising residues 1583–1620. The peptide was not a stable coiled coil, but instead displayed random coil secondary structure with some α-helical content as measured by negative ellipticity at 200 nm with a shoulder at 222 nm, respectively (Fig. 3*C*). In contrast, the longer fragment of TRIP230 comprising residues 1583–1688 had a circular dichroism spectrum consistent with coiled coil structure, indicated by equal minima at 208 and 222 nm ($\theta_{222}/\theta_{208} = 1.005$) (37). Truncation of the C-terminal coiled coil element from residues 1663–1688 resulted in loss of coiled coil structure in all TRIP230 peptides (supplemental Fig. S3), demonstrating that this region is important for coiled coil formation or stability. However, peptides of the length required to maintain coiled coil formation (residues 1663–1688) and the ARNT interaction motif (residues 1583–1620) were not optimal for NMR, displaying poor chemical shift dispersion and peak intensities (data not shown). We therefore focused on characterizing the $TRIP230^{1583-1620}$ peptide and obtained full backbone chemical shift assignments complemented by partial side-chain assignments. Analysis of $^{13}C\alpha$ chemical shifts ($\Delta\delta = \Delta\delta_{obs} - \Delta\delta_{random\ coil}$) (38) in

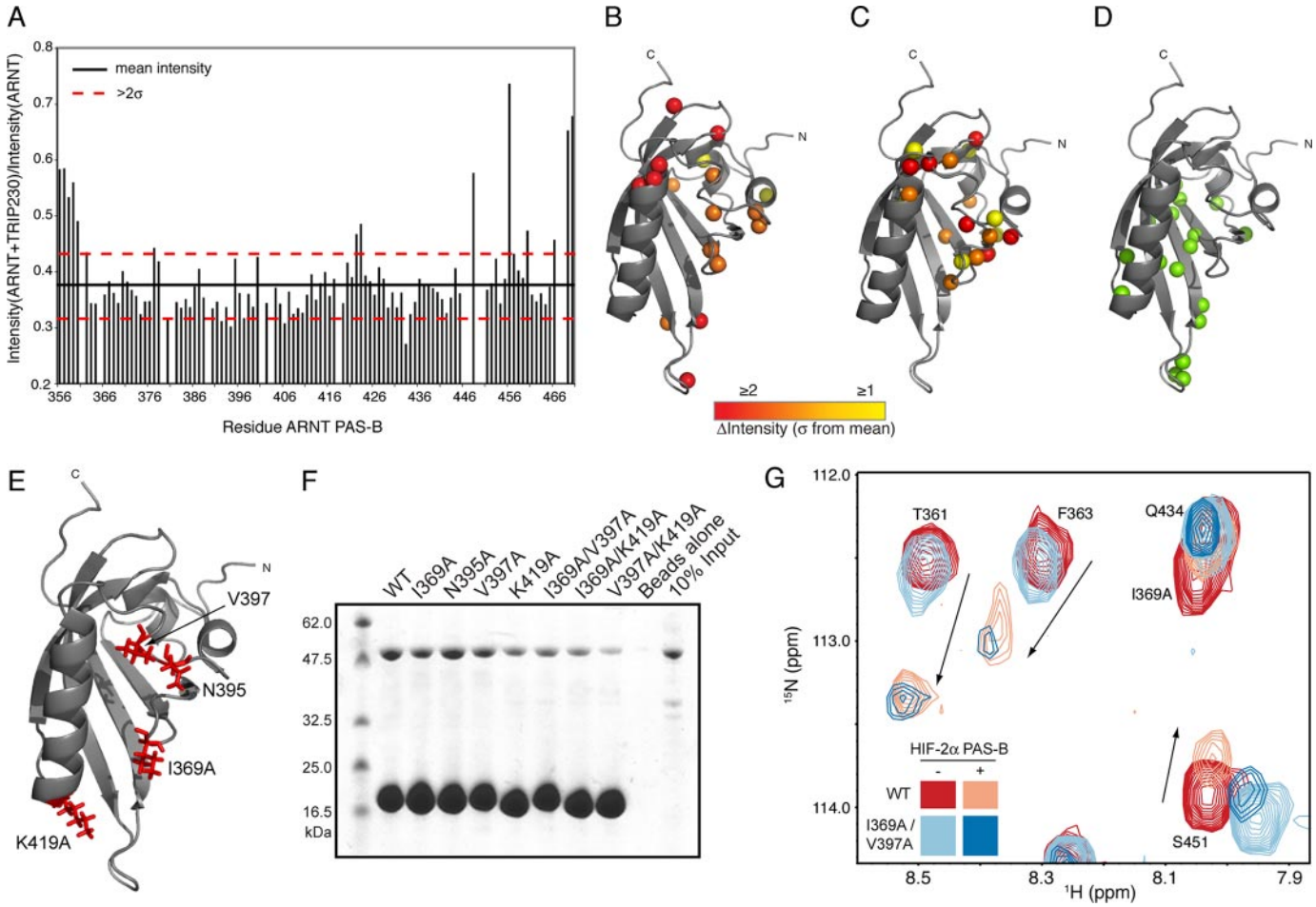

FIGURE 2. **Mapping the coiled coil interaction interface on ARNT PAS-B.** *A*, intermediate exchange-mediated line broadening of 200 μM U-^{15}N ARNT PAS-B was quantified for all well resolved peaks in the absence and presence of 100 μM TRIP230$^{1583-1688}$. Mean peak intensity is plotted with the *black line*, and the 2σ significance cutoff is shown with the *dashed red lines*. *B*, TRIP230$^{1583-1688}$ binding mapped on the ARNT PAS-B structure. *Spheres* represent backbone amides exhibiting significant broadening, in order of increasing effect from *yellow* to *red*. *C*, CoCoA$^{407-535}$ binding mapped on the ARNT PAS-B structure. *Spheres* represent amide protons indicated as above. *D*, HIF-2α PAS-B binding mapped on the ARNT PAS-B structure. *Green spheres* represent amide protons for which $\Delta\delta_{TOT}$>0.05 ppm upon addition of 500 μM HIF-2α PAS-B to 250 μM U-^{15}N ARNT PAS-B (10). *E*, residues chosen for alanine mutation on the ARNT PAS-B α-helical face mapped onto the PAS-B structure. *F*, pull-down assay of His$_6$-tagged WT and mutant ARNT PAS-B domains with GST-TRIP$^{1583-1688}$. *G*, heterodimerization of HIF-2α PAS-B with WT or I369A/V397A U-^{15}N ARNT PAS-B. 320 μM HIF-2α PAS-B was added to 160 μM U-^{15}N ARNT PAS-B WT or I369A/V397A and binding was monitored by ^{15}N/^{1}H HSQC spectra. *Arrows* illustrate similar HIF-2α PAS-B-induced chemical shift perturbations in both WT and I369A/V397A ARNT PAS-B.

TRIP230$^{1583-1620}$ show a trend toward $\Delta\delta > 0$ for residues 1594–1610, suggesting α-helix (Fig. 3*D*). This is in agreement with more comprehensive TALOS analysis, which uses ^{15}N, ^{13}CO, ^{13}Cβ, and ^{1}Hα chemical shifts to predict secondary structure (*bar over plot* in Fig. 3*D*) (39).

Mapping ARNT PAS-B Binding on TRIP230 Minimal Fragment by NMR—We then used NMR titration experiments to define the ARNT-interacting region on TRIP230$^{1583-1620}$. 100 μM U-^{15}N/^{13}C-labeled TRIP230$^{1583-1620}$ was incubated with ARNT PAS-B (from 50–900 μM, in 6 steps) and binding was monitored by ^{15}N/^{1}H HSQC spectra. Selected amide peaks in the N terminus of the peptide exhibited both broadening and chemical shift changes in the ^{15}N/^{1}H HSQC (Fig. 4*A*), while a similar titration experiment performed with the HIF-2α PAS-B showed no significant chemical shift or peak intensity changes (supplemental Fig. S4). A highlighted region of the ^{15}N/^{1}H HSQC spectra containing residues Leu-1588, Leu-1589, and the last residue of vector-derived sequence (a Val at position 17, V*17) (Fig. 4*B*) showed chemical shift perturbations and broadening while residues at the C-terminal end of the peptide were essentially unaffected. These are consistent with our pull-down data, which established that the first 10 residues of this peptide contain the important determinants of ARNT binding. We also obtained ^{13}C/^{1}H HSQC spectra at each of the titration points to monitor changes in TRIP230 side chains affected by ARNT PAS-B. Consistent with the ^{15}N/^{1}H HSQC data, well resolved ^{13}Cα/^{1}Hα peaks of residues at the N terminus of the peptide (V*17Cα, S1594Cα, and T1596Cα) were significantly broadened while others in the C terminus (V1613Cα, T1614Cα) or vector-derived extreme N terminus (P*5Cα) of the peptide were unaffected (Fig. 4*C*).

Identification of Conserved LXXXLL Motif as the ARNT PAS-B Interaction Motif—ARNT-induced backbone chemical shift changes were mapped by residue onto the TRIP230$^{1583-1620}$ peptide sequence (Fig. 5*A*). We noted a distinct periodicity of chemical shift perturbation in the N terminus of the peptide occurring every 3–4 residues. Although this region is disordered in the apo protein, the periodicity of perturbed residues suggested formation of α-helix upon binding ARNT PAS-B. A helical wheel projection of the first 18 residues of the peptide is

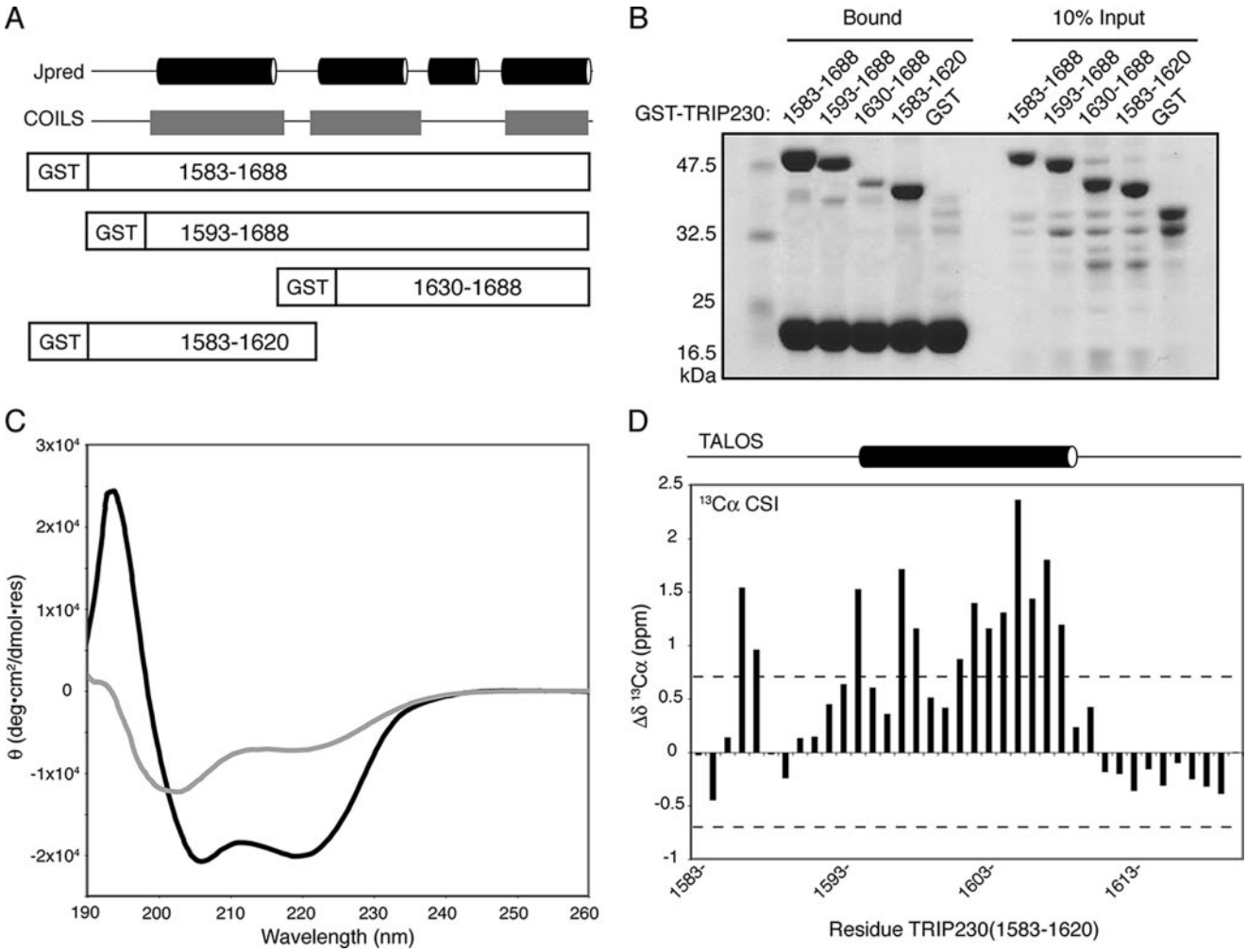

FIGURE 3. **Structural characterization of the ARNT-binding domain of TRIP230.** *A*, schematic representation of TRIP230 truncation fragments with Jpred secondary structure (48) and COILS coiled coil (49) predictions indicated above in *black* or *gray bars*, respectively. *B*, pull-down assay of His_6-tagged ARNT PAS-B with GST-tagged TRIP230 fragments. *C*, circular dichroism spectra of TRIP230 peptides. Far-UV CD spectra of 15 μM $TRIP230^{1583-1620}$, in *gray*, and $TRIP230^{1583-1688}$, in *black*, were recorded at pH 6.5 (25 °C). *D*, secondary structure determination from $^{13}C\alpha$ chemical shift comparison. $TRIP230^{1583-162013}C\alpha$ shifts were compared against the Chemical Shift Index (38), with significant deviation from random coil set to $\pm$ 0.7 ppm. TALOS prediction of secondary structure from $TRIP230^{1583-1620}$ chemical shifts is indicated above the plot in schematic form (39).

consistent with formation of an amphipathic α-helix (Fig. 5*B*), with residues showing the greatest ARNT-induced perturbations mapping to the largely hydrophobic face of the helix. Notably, this region contains an L*XX*LL-like nuclear receptor (NR) box (LRNHLL) located within the N terminus and on the hydrophobic face of the peptide. L*XXX*LL motifs function similarly to NR boxes in mediating transcription factor/coactivator interactions (40). Alignment of TRIP230 sequences within this region shows that residues within the ARNT interaction motif we identified are highly conserved across insect and vertebrate animal species (*underline*, Fig. 5*C*).

Mutation of ARNT PAS-B Interaction Motif on TRIP230 Attenuates Binding—To assess the functional importance of the L*XXX*LL motif, we serially mutated tandem residue pairs within this motif to alanine (Fig. 5*D*) and monitored their effect on ARNT PAS-B binding by pull-down assay (Fig. 5*E*). Mutation of Site 1 to create an L*XXX*AA motif significantly decreased binding to ARNT PAS-B, consistent with previous loss-of-function mutations of LL sequences in NR boxes (41). Residues adjacent to NR boxes are often critical for determining the specificity and affinity of binding (42, 43). We mutated conserved residues on the largely hydrophobic face of the amphipathic helix containing the L*XXX*LL motif. While the backbone amides of some of these residues did not exhibit significant backbone chemical shift changes in the $^{15}N/^{1}H$ HSQC-monitored titration with ARNT PAS-B, significant broadening was observed for side chain atoms of residues Asp-1593 and Thr-1596 in $^{13}C/^{1}H$ HSQC spectra (supplemental Fig. S5). Mutation of Site 2 (E1592A/D1593A) decreased PAS-B binding, demonstrating that the interruption of hydrophobicity within the amphipathic helix by these residues may be a functionally important feature. Mutation of Site 3 (Y1595A/T1596A) also decreased binding, consistent with an important role for residues within the preformed α-helix in maintaining the interaction with ARNT PAS-B upon loss of the first ten residues (Fig. 3*B* and the ΔN10 fragment in Fig. 5*E*). Furthermore, these data are consistent with quantitative measurements of the affinity between ARNT PAS-B and TRIP230 fragments as measured using AlphaScreen®, a bead-based luminescence proximity assay we engineered to report on the

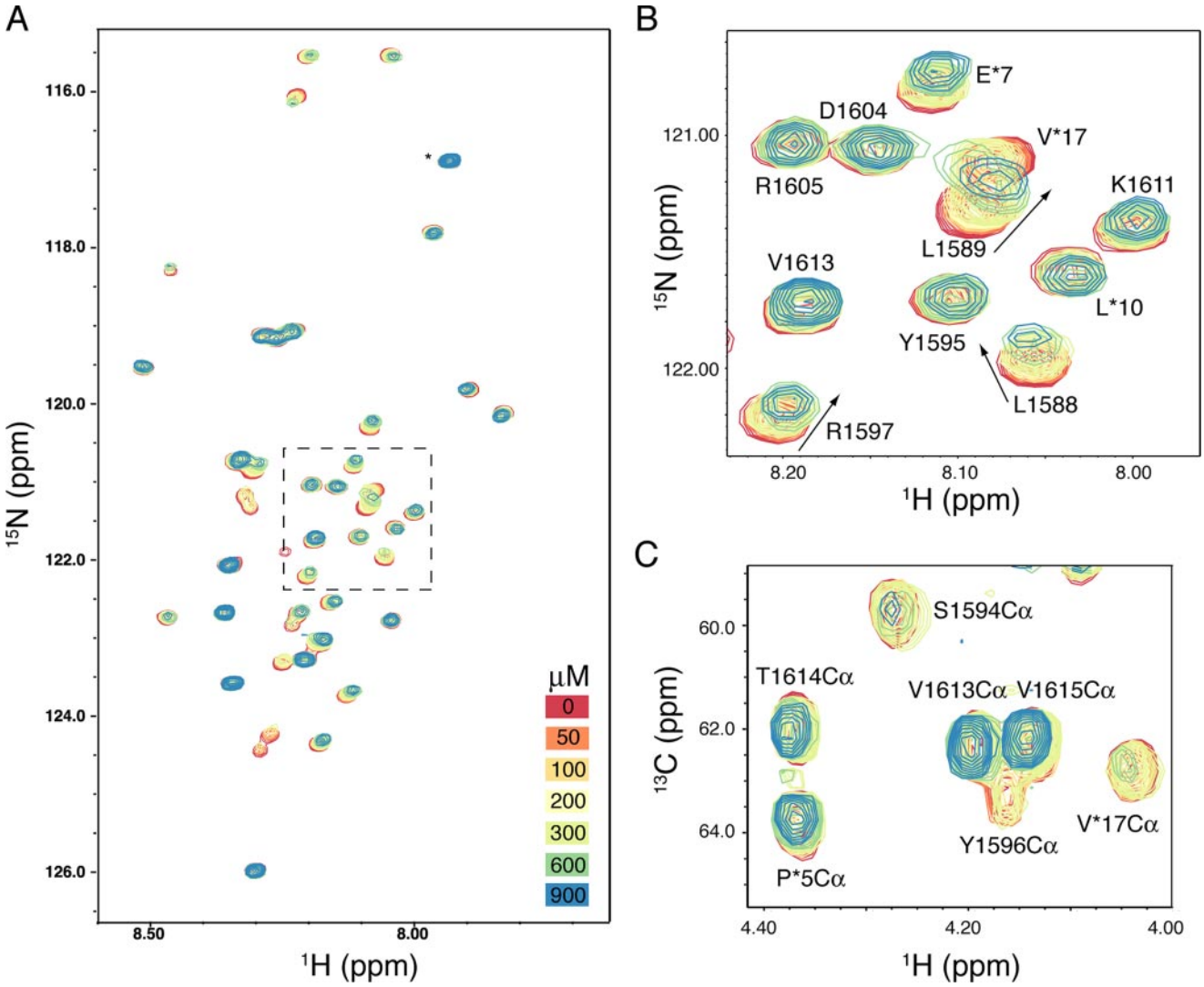

FIGURE 4. **Mapping the ARNT PAS-B interaction interface on the TRIP230 minimal peptide.** *A*, $^{15}N/^{1}H$ HSQC spectra of the titration of 100 μM U-^{15}N/TRIP230$^{1583-1620}$ with 50–900 μM ARNT PAS-B. *, peak is aliased from its true position at 130.3 ^{15}N ppm. *B*, highlighted region of $^{15}N/^{1}H$ HSQC titration showing chemical shift perturbation and intermediate exchange-mediated line broadening of N-terminal residues. Residues from the vector-derived N terminus are listed as residue* position (E*7). *C*, $^{13}C/^{1}H$ HSQC spectra of the titration of 100 μM U-$^{15}N/^{13}C$ TRIP230$^{1583-1620}$ with 50–900 μM ARNT PAS-B. Residues with well resolved $^{13}C\alpha/^{1}H\alpha$ peaks are shown, demonstrating significant peak broadening of N-terminal residues.

interaction of a FLAG-tagged ARNT PAS-B and GST-tagged TRIP230 proteins. Titrating GST-TRIP230 fragments into samples of ARNT PAS-B-FLAG, we obtained a K_d of ~65 nM for the ARNT·TRIP230$^{1583-1688}$ complex. Mutation at Site 1 (K_d ~ 970 nM) or deletion of the N-terminal 10 amino acids (K_d ~ 3900 nM) significantly decreased the strength of this interaction by ~1.7–2.5 kcal/mol (supplemental Fig. S6). Collectively, these data support a role for an L*XXX*LL motif and adjacent residues within the coiled coil coactivator TRIP230 in interacting with the α-helical face of ARNT PAS-B.

DISCUSSION

Simultaneous recruitment of multiple coactivators by different domains within transcription factor complexes is important for transcriptional activation, whereby interactions of varying stability are important for determining specificity of gene induction and cross-talk with other pathways (44, 45). Within the bHLH-PAS family, the use of C-terminal activation domains to recruit coactivators is well documented (13–15), but PAS domains have also been shown to contribute to the specificity of gene induction (22), suggesting that they too interact with coactivators. Recent reports of coiled coil coactivators that target the N-terminal bHLH and/or PAS domains of ARNT (18, 20, 21) support a role for ARNT in transcriptional activation in the absence of a functional C-TAD (16, 17). Here we show that ARNT interacts with the coiled coil coactivators TRIP230 and CoCoA through a single PAS domain, utilizing the same α-helical face to interact with both coactivators.

The ARNT PAS-B domain makes critical interactions with its heterodimeric partner HIF-2α that are required for the stability and activity of the HIF-2 complex *in vivo* (8, 9), and we demonstrated here that ARNT PAS-B is the primary site of interaction for coiled coil coactivators. Although the ARNT PAS-A domain did not appear to contain a high affinity coactivator binding site, nor did it cooperatively enhance coactivator binding by ARNT PAS-B within a tandem PAS-AB construct, we cannot rule out the possibility that coactivators make weak

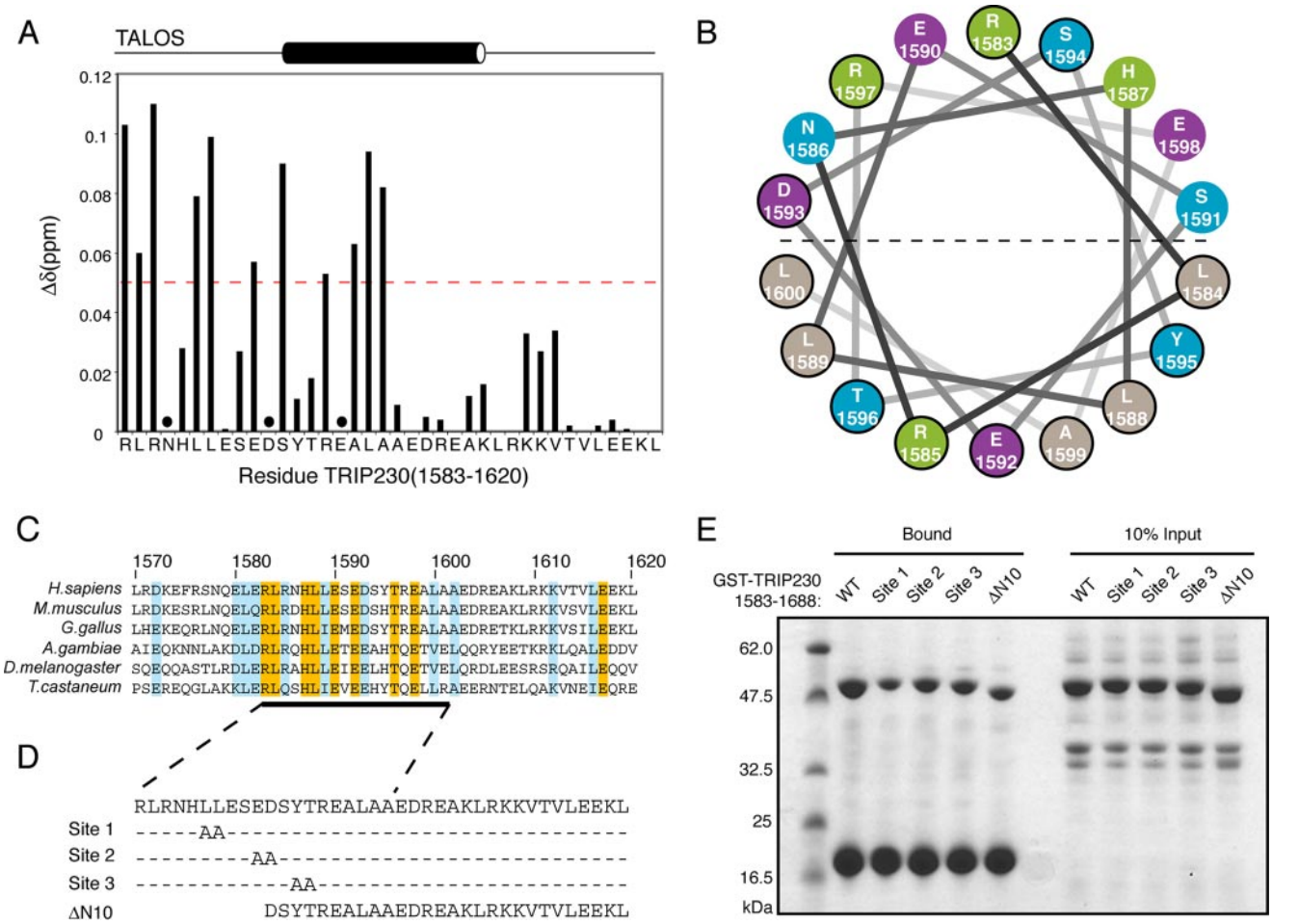

FIGURE 5. **A conserved L*XXX*LL motif on TRIP230 mediates interaction with ARNT PAS-B.** *A*, $^{1}H,^{15}N$ amide chemical shift perturbation of TRIP230 by ARNT PAS-B. $\Delta\delta_{TOT}$ for all well resolved peaks within the TRIP230$^{1583-1620}$ peptide are displayed with a $\Delta\delta_{TOT} = 0.05$ ppm significance cutoff (*dashed line*). Residues with weak or overlapping peaks (●) were not included in the analysis. *B*, helical wheel projection of TRIP230 residues 1583–1600. Residues are notated as the single amino acid code and peptide numbering (beginning with residue 1583), and those with significant $\Delta\delta_{TOT}$ or chemical shift broadening are outlined in *black*. Coloring scheme: polar/charged, *green* or *purple*; polar/uncharged, *blue*; nonpolar, *beige*. *C*, alignment of TRIP230 protein sequences containing the ARNT-interaction motif (*underlined*). Residues conserved 100% from insect to humans are colored *yellow*, while highly conserved/similar residues are colored *light blue*. *D*, mutation of ARNT-interacting motif in TRIP230. Sequences of site 1–3 mutants and the ΔN10 fragment (GST-TRIP230$^{1593-1688}$) are schematically shown. *E*, pull-down assay of His$_6$-tagged ARNT PAS-B with GST-tagged TRIP230$^{1583-1688}$ WT and mutant or truncated peptides.

or transient interactions with ARNT PAS-A. However, our data suggest a model in which the ARNT PAS-B domain is critically important for hypoxia signaling, simultaneously mediating heterodimer formation with HIF-2α on its β-sheet and using its opposing α-helical face to recruit coactivators such as TRIP230 that are required for transcriptional responses (18, 20). We tested for formation of the HIF-2α PAS-B·ARNT PAS-B·TRIP230 heterotrimer in our pull-down assays but were unable to detect the complex *in vitro*, most likely due to the relatively weak affinity of the two isolated PAS-B domains for one another (8, 11).

The use of L*XX*LL-like motifs to mediate transcription factor-coactivator interactions is widespread; these short, linear motifs bind their cognate receptors with low to moderate affinity, ideal for transient signaling interactions (46). Furthermore, disorder to order transitions in L*XX*LL-like motifs upon binding appears to be another way to achieve specificity with lower affinity (reviewed in Ref. 47). Our TALOS secondary structure analysis indicates that the TRIP230$^{1583-1620}$ L*XXX*LL motif is disordered in the apo state, while the periodicity of chemical shift perturbations suggests that it forms a helix upon interaction with ARNT, supporting the idea that binding to ARNT induces helical structure in the TRIP230 L*XXX*LL motif. Furthermore, residues proximal to L*XX*LL-like motifs are often critical for determining the affinity of binding (42, 43). Based on our mutation and quantitative binding data, residues C-terminal to the TRIP230$^{1583-1620}$ L*XXX*LL motif are also important for binding to ARNT PAS-B. While the specific ARNT interaction motif of CoCoA was not identified in the present study, it is interesting to speculate whether a motif with similar helical and charge propensities will mediate that interaction as well.

We note remarkable similarities of the ARNT PAS-B·TRIP230 interaction with complex formation of the SRC-1 PAS-B with different L*XX*LL motifs that use the same PAS α-helical interface (23, 24). Of particular interest is the unique structure of the SRC-1 PAS-B domain in its co-crystal structure with a STAT-6 peptide (24), an inverse of typical signaling logic where the PAS-B domain of the SRC-1 coactivator interacts with the L*XX*LL motif of the STAT-6 transcription factor. The α-helical face of the SRC-1 PAS-B domain has undergone dra-

matic rearrangement from the three short α-helices seen in a prototypical PAS domain into a single long α-helix that contacts the L*XX*LL motif of STAT-6, and is the only known PAS domain structure to have this unique α-helical arrangement (24). We currently have no evidence for specific structural rearrangements on ARNT PAS-B as a result of coactivator binding, precluded to a large degree by broadening of PAS-B peaks upon interaction with TRIP230 and CoCoA. Further structural studies will possibly resolve whether coactivator binding by ARNT is coupled to a similar structural rearrangement of its α-helical interface.

In conclusion, this study highlights the versatility of small modular domains that mediate protein-protein interactions within larger complexes. ARNT uses its small, 14-kDa PAS-B domain to simultaneously coordinate two sets of protein interactions that are critical for transcriptional responses to hypoxia by using interfaces on opposing sides of the domain. The recruitment of different coactivators by the TADs of HIF-α and the PAS-B domain of ARNT likely contributes to the combinatorial nature of transcriptional activation leading to a diverse array of transcriptional responses to a given stimulus. Further regulation of this response by environmental factors could provide additional temporal or tissue-specific regulation of transcriptional responses.

REFERENCES

1. Taylor, B. L., and Zhulin, I. B. (1999) *Microbiol. Mol. Biol. Rev.* **63,** 479–506
2. Crews, S. T., and Fan, C. M. (1999) *Curr. Opin. Genet. Dev.* **9,** 580–587
3. Kewley, R. J., Whitelaw, M. L., and Chapman-Smith, A. (2004) *Int. J. Biochem. Cell Biol.* **36,** 189–204
4. Andersson, P., McGuire, J., Rubio, C., Gradin, K., Whitelaw, M. L., Pettersson, S., Hanberg, A., and Poellinger, L. (2002) *Proc. Natl. Acad. Sci. U. S. A.* **99,** 9990–9995
5. Maxwell, P. H., Dachs, G. U., Gleadle, J. M., Nicholls, L. G., Harris, A. L., Stratford, I. J., Hankinson, O., Pugh, C. W., and Ratcliffe, P. J. (1997) *Proc. Natl. Acad. Sci. U. S. A.* **94,** 8104–8109
6. Chapman-Smith, A., Lutwyche, J. K., and Whitelaw, M. L. (2004) *J. Biol. Chem.* **279,** 5353–5362
7. Chapman-Smith, A., and Whitelaw, M. L. (2006) *J. Biol. Chem.* **281,** 12535–12545
8. Erbel, P. J., Card, P. B., Karakuzu, O., Bruick, R. K., and Gardner, K. H. (2003) *Proc. Natl. Acad. Sci. U. S. A.* **100,** 15504–15509
9. Yang, J., Zhang, L., Erbel, P. J., Gardner, K. H., Ding, K., Garcia, J. A., and Bruick, R. K. (2005) *J. Biol. Chem.* **280,** 36047–36054
10. Card, P. B., Erbel, P. J., and Gardner, K. H. (2005) *J. Mol. Biol.* **353,** 664–677
11. Scheuermann, T. H., Tomchick, D. R., Machius, M., Guo, Y., Bruick, R. K., and Gardner, K. H. (2009) *Proc. Natl. Acad. Sci. U. S. A.* **106,** 450–455
12. Perissi, V., and Rosenfeld, M. G. (2005) *Nat. Rev. Mol. Cell Biol.* **6,** 542–554
13. Dayan, F., Roux, D., Brahimi-Horn, M. C., Pouyssegur, J., and Mazure, N. M. (2006) *Cancer Res.* **66,** 3688–3698
14. Gu, J., Milligan, J., and Huang, L. E. (2001) *J. Biol. Chem.* **276,** 3550–3554
15. Ma, Q., Dong, L., and Whitlock, J. P., Jr. (1995) *J. Biol. Chem.* **270,** 12697–12703
16. Ko, H. P., Okino, S. T., Ma, Q., and Whitlock, J. P., Jr. (1996) *Mol. Cell. Biol.* **16,** 430–436
17. Li, H., Ko, H. P., and Whitlock, J. P. (1996) *J. Biol. Chem.* **271,** 21262–21267
18. Beischlag, T. V., Taylor, R. T., Rose, D. W., Yoon, D., Chen, Y., Lee, W. H., Rosenfeld, M. G., and Hankinson, O. (2004) *J. Biol. Chem.* **279,** 54620–54628
19. Chen, Y. H., Kim, J. H., and Stallcup, M. R. (2005) *Mol. Cell. Biol.* **25,** 5965–5972
20. Kim, J. H., and Stallcup, M. R. (2004) *J. Biol. Chem.* **279,** 49842–49848
21. Sadek, C. M., Jalaguier, S., Feeney, E. P., Aitola, M., Damdimopoulos, A. E., Pelto-Huikko, M., and Gustafsson, J. A. (2000) *Mech. Dev.* **97,** 13–26
22. Zelzer, E., Wappner, P., and Shilo, B. Z. (1997) *Genes Dev.* **11,** 2079–2089
23. Lodrini, M., Munz, T., Coudevylle, N., Griesinger, C., Becker, S., and Pfitzner, E. (2008) *Nucleic Acids Res.* **36,** 1847–1860
24. Razeto, A., Ramakrishnan, V., Litterst, C. M., Giller, K., Griesinger, C., Carlomagno, T., Lakomek, N., Heimburg, T., Lodrini, M., Pfitzner, E., and Becker, S. (2004) *J. Mol. Biol.* **336,** 319–329
25. Harper, S. M., Neil, L. C., and Gardner, K. H. (2003) *Science* **301,** 1541–1544
26. Sheffield, P., Garrard, S., and Derewenda, Z. (1999) *Protein Expr. Purif.* **15,** 34–39
27. Blommel, P. G., and Fox, B. G. (2007) *Protein Expr. Purif.* **55,** 53–68
28. Gasteiger, E., Hoogland, C., Gattiker, A., Duvaud, S., Wilkins, M. R., Appel, R. D., and Bairoch, A. (2005) in *The Proteomics Protocols Handbook* (Walker, J. M. ed) pp. 571–607, Humana Press
29. Johnson, B. A. (2004) *Methods Mol. Biol.* **278,** 313–352
30. Farmer, B. T., 2nd, Constantine, K. L., Goldfarb, V., Friedrichs, M. S., Wittekind, M., Yanchunas, J., Jr., Robertson, J. G., and Mueller, L. (1996) *Nat. Struct. Biol.* **3,** 995–997
31. Cavanagh, J., Fairbrother, W. J., Palmer III, A. G., Skelton, N. J., and Rance, M. (2006) *Protein NMR Spectroscopy: Principles and Practice*, 2nd Ed., pp. 535–673, Academic Press
32. Pascal, S. M., Muhandiram, D. R., Yamazaki, T., Forman-Kay, J. D., and Kay, L. E. (1994) *J. Magn. Resonance, Series B* **103,** 197–201
33. Delaglio, F., Grzesiek, S., Vuister, G. W., Zhu, G., Pfeifer, J., and Bax, A. (1995) *J. Biomol. NMR* **6,** 277–293
34. Larkin, M. A., Blackshields, G., Brown, N. P., Chenna, R., McGettigan, P. A., McWilliam, H., Valentin, F., Wallace, I. M., Wilm, A., Lopez, R., Thompson, J. D., Gibson, T. J., and Higgins, D. G. (2007) *Bioinformatics* **23,** 2947–2948
35. Chang, K. H., Chen, Y., Chen, T. T., Chou, W. H., Chen, P. L., Ma, Y. Y., Yang-Feng, T. L., Leng, X., Tsai, M. J., O'Malley, B. W., and Lee, W. H. (1997) *Proc. Natl. Acad. Sci. U. S. A.* **94,** 9040–9045
36. Kim, J. H., Li, H., and Stallcup, M. R. (2003) *Mol. Cell* **12,** 1537–1549
37. Graddis, T. J., Myszka, D. G., and Chaiken, I. M. (1993) *Biochemistry* **32,** 12664–12671
38. Wishart, D. S., and Sykes, B. D. (1994) *J. Biomol. NMR* **4,** 171–180
39. Cornilescu, G., Delaglio, F., and Bax, A. (1999) *J. Biomol. NMR* **13,** 289–302
40. Zwijsen, R. M., Buckle, R. S., Hijmans, E. M., Loomans, C. J., and Bernards, R. (1998) *Genes Dev.* **12,** 3488–3498
41. Heery, D. M., Kalkhoven, E., Hoare, S., and Parker, M. G. (1997) *Nature* **387,** 733–736
42. Chang, C., Norris, J. D., Gron, H., Paige, L. A., Hamilton, P. T., Kenan, D. J., Fowlkes, D., and McDonnell, D. P. (1999) *Mol. Cell. Biol.* **19,** 8226–8239
43. Suzuki, T., Kasahara, M., Yoshioka, H., Morohashi, K., and Umesono, K. (2003) *Mol. Cell. Biol.* **23,** 238–249
44. Marr, M. T., 2nd, Isogai, Y., Wright, K. J., and Tjian, R. (2006) *Genes Dev.* **20,** 1458–1469
45. McKenna, N. J., Nawaz, Z., Tsai, S. Y., Tsai, M. J., and O'Malley, B. W. (1998) *Proc. Natl. Acad. Sci. U. S. A.* **95,** 11697–11702
46. Savkur, R. S., and Burris, T. P. (2004) *J. Pept. Res.* **63,** 207–212
47. Wright, P. E., and Dyson, H. J. (1999) *J. Mol. Biol.* **293,** 321–331
48. Cole, C., Barber, J. D., and Barton, G. J. (2008) *Nucleic Acids Res.* **36,** W197–201
49. Lupas, A., Van Dyke, M., and Stock, J. (1991) *Science* **252,** 1162–1164

SUPPLEMENTAL FIGURE LEGENDS

Supp. Figure S1 I369A/V397A mutation of ARNT PAS-B induces chemical shift perturbations localized to α-helical face. *A*, Overlaid $^{15}N/^{1}H$ HSQC spectra from 160 μM WT (black) or I369A/V397A (red) ARNT PAS-B, showing minimal chemical shift perturbations indicative of a well-folded PAS-B domain. *B*, Chemical shift perturbations (cyan) are mapped onto the ARNT PAS-B structure. I369A and V397A mutations are shown in red.

Supp. Figure S2 Interaction of additional TRIP230 fragments with ARNT PAS-B. Pull-down assay of His_6-tagged ARNT PAS domains with GST-tagged TRIP230 fragments. Bound proteins were analyzed by Coomassie stain of SDS-PAGE. * indicates GST-truncation product (containing full-length TRIP230 fragment) that bind to PAS domains. MW of ARNT PAS constructs: His_6Gβ1 ARNT PAS-A, 32.0 kDa; His_6 ARNT PAS-B, 13.6 kDa; His_6 ARNT PAS-AB, 35.6 kDa. A schematic of TRIP230 fragment secondary structure and coiled coil propensity is shown below. The N-terminal region of the $TRIP230^{1583-1716}$ interacts with ARNT PAS-B and ARNT PAS-AB, while residues 1663-1716 do not interact with ARNT.

Supp. Fig. S3 Circular dichroism of additional TRIP230 peptides. Far-UV CD spectra of 15 μM TRIP230 peptides were recorded at pH 6.5 (25ºC). Note loss of coiled coil structure (demonstrated by equal ellipticity minima at 208 and 222 nm) with truncation of residues 1663-1716, suggesting that these residues are important for coiled coil formation and/or stability.

Supp. Fig. S4 Titration of U-$^{15}N/^{13}C$ $TRIP230^{1583-1620}$ with HIF-2α PAS-B. $^{15}N/^{1}H$ HSQC spectra of the titration of 100 μM U-$^{15}N/^{13}C$ $TRIP230^{1583-1620}$ with 50-900 μM HIF-2α PAS-B. * peak is aliased from its true position at 130.3 ^{15}N ppm. Mean peak intensity (^{15}N $TRIP^{1583-1620}$/^{15}N $TRIP^{1583-1620}$ + 900μM HIF-2α PAS-B) = 0.82 ± 0.072 with no peaks broadened > 1σ.

Supp. Fig. S5 Chemical shift broadening of TRIP230 resonances upon titration of ARNT PAS-B. Highlighted regions of $^{13}C/^{1}H$ HSQC spectra of the titration of 100 μM U-$^{15}N/^{13}C$ $TRIP230^{1583-1620}$ with 50-900 μM ARNT PAS-B. Residues with well resolved $^{13}C\alpha/^{1}H\alpha$ peaks are shown, demonstrating significant peak broadening of N-terminal residues.

Supp. Fig. S6 Determination of ARNT PAS-B•GST-coactivator binding affinities by AlphaScreen® assay. *A*, Binding curves for GST-$TRIP230^{1593-1688}$ WT in the presence (red) or absence (orange) of 25 nM ARNT PAS-B-FLAG. Error bars represent triplicate data points within each assay (2 independent assays performed). A negative control of GST alone (blue) with 25 nM ARNT PAS-B-FLAG was also performed, giving rise to counts that were similar to beads alone (data not shown). *B*, Binding curves for the GST-$TRIP230^{1583-1688}$ Site 1 mutant or GST-$TRIP230^{1593-1688}$ (ΔN10) fragment in the presence or absence of 25 nM ARNT PAS-B-FLAG, as well as a titration with GST alone (green).

C, Calculated dissociation constants from nonlinear fitting of binding data to a one site binding equation (hyperbola) in GraphPad Prism 5.0a.

A

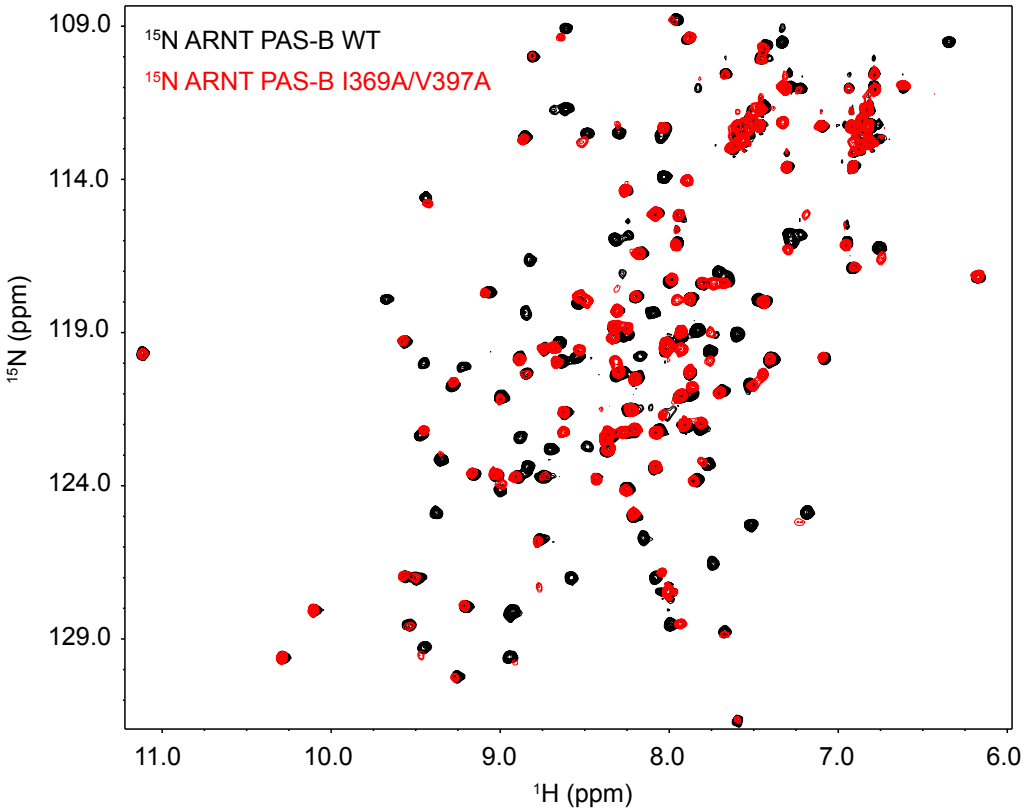

B

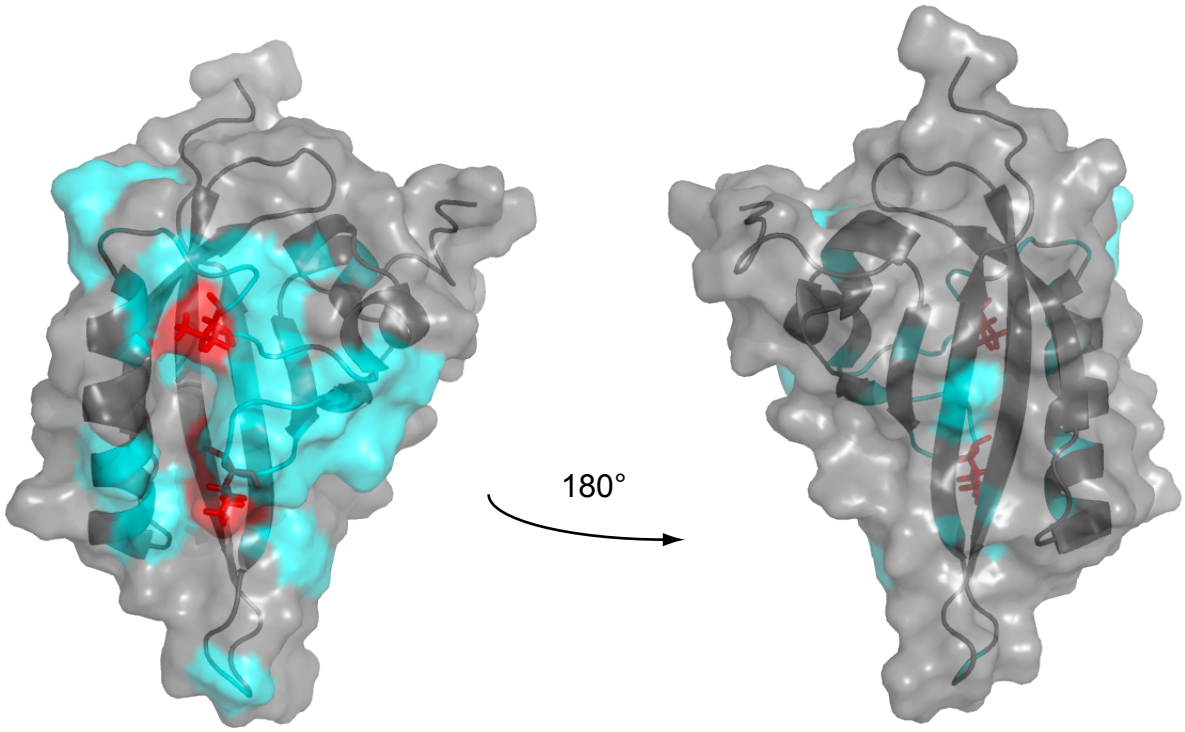

Supplemental Figure S1

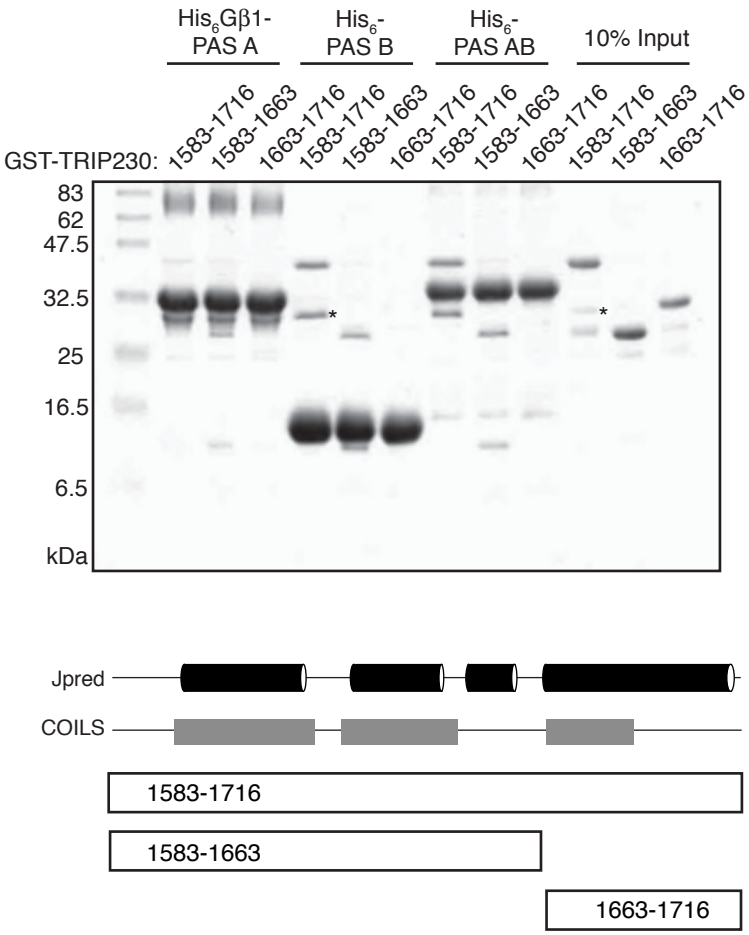

Supplemental Figure S2

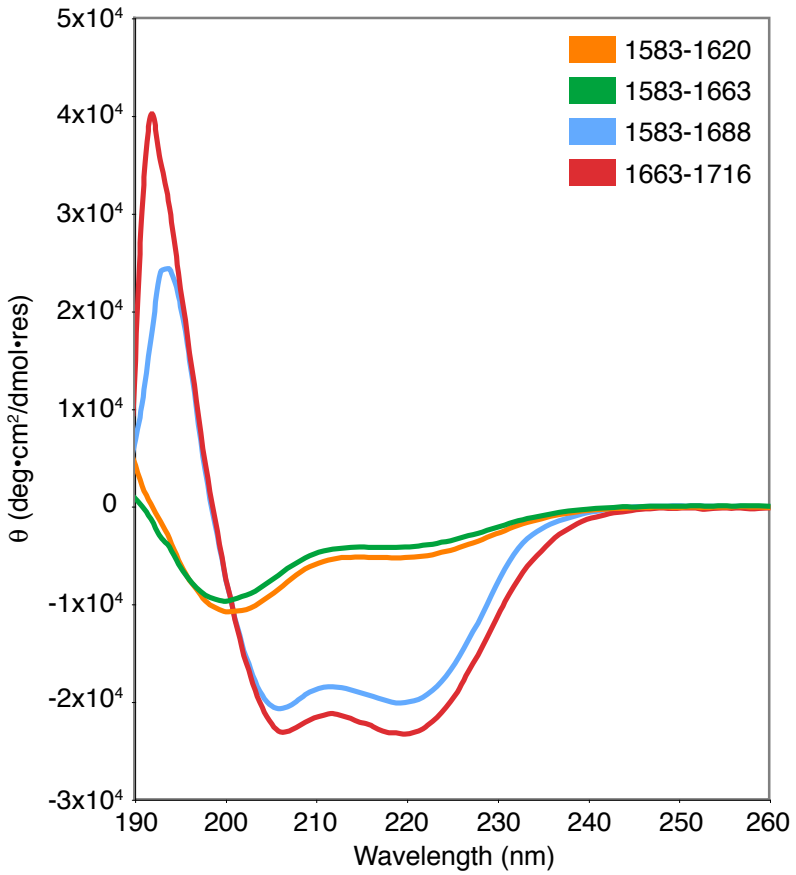

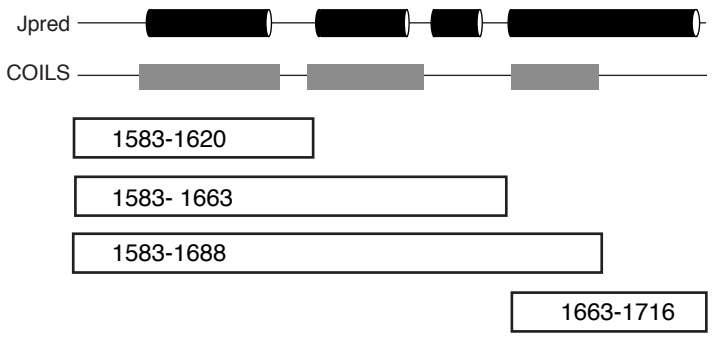

Supplementary Figure S3

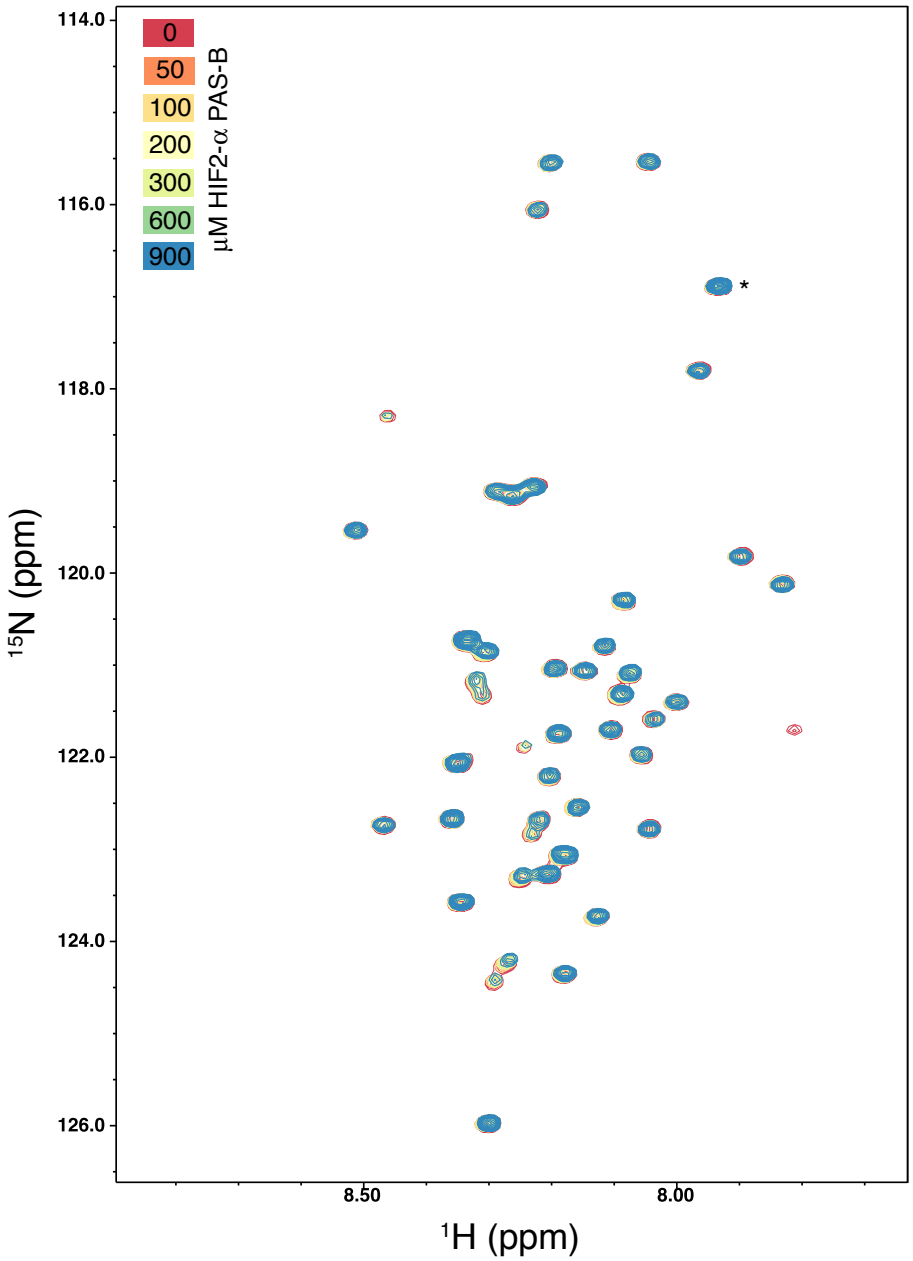

Supplementary Figure S4

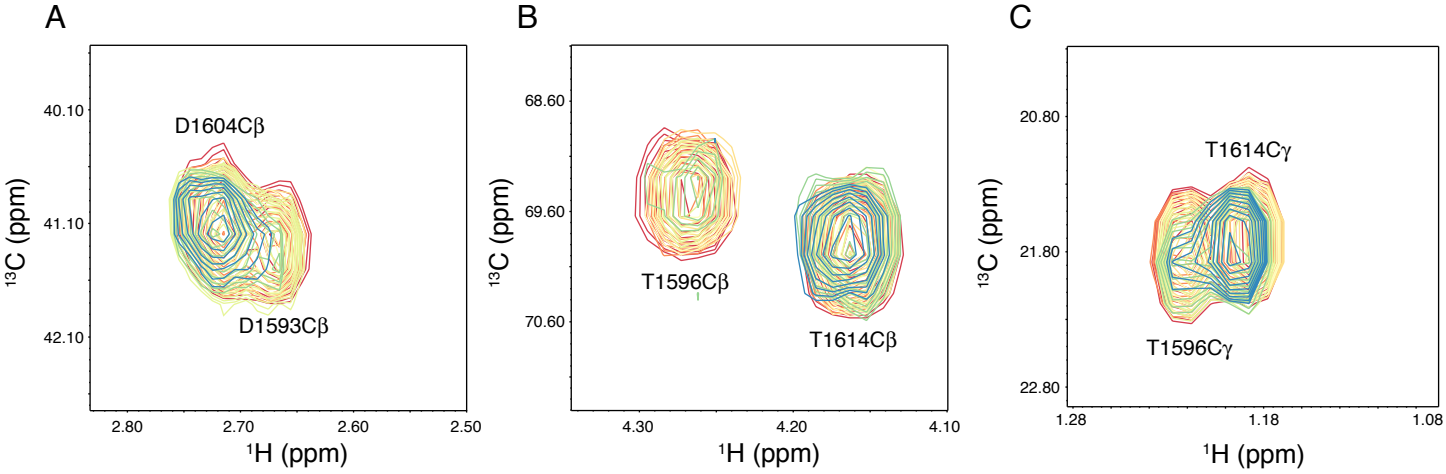

Supplemental Figure S5

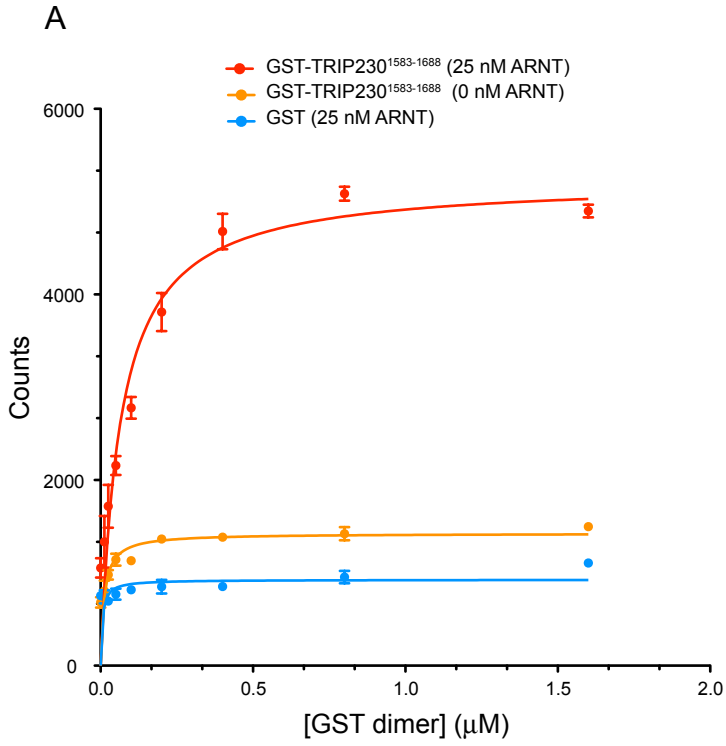

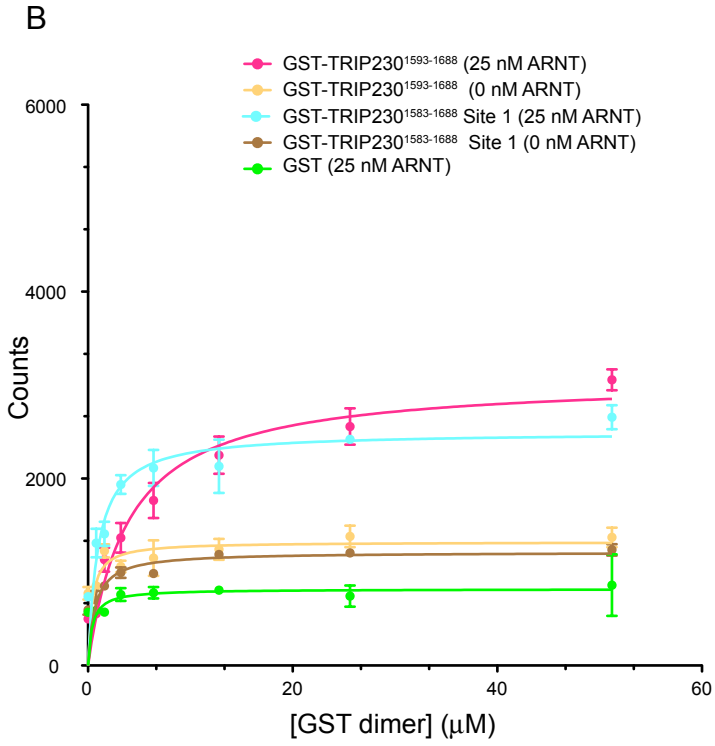

C

	K_d
GST-TRIP230$^{1583-1688}$	64.8 ± 11.1 nM
GST-TRIP230$^{1583-1688}$ Site 1	0.97 ± 0.29 μM
GST-TRIP230$^{1593-1688}$ (ΔN10)	3.9 ± 0.79 μM

Supplemental Figure S6